HHS Public Access

Endothelial struts enable the generation of large lumenized blood vessels *de novo*

Bart Weijts[1,4,*], **Iftach Shaked**[2], **Mark Ginsberg**[3], **David Kleinfeld**[2], **Catherine Robin**[4,5], **David Traver**[1,*]

[1]Section of Cell and Developmental Biology, Division of Biological Sciences, University of California-San Diego, La Jolla, CA 92093, USA

[2]Department of Physics, University of California at San Diego, La Jolla, CA 92093, USA; Section of Neurobiology, University of California at San Diego, La Jolla, CA 92093, USA

[3]Department of Medicine, University of California, San Diego, La Jolla, CA.

[4]Hubrecht Institute-KNAW & University Medical Center Utrecht, 3584 CT Utrecht, The Netherlands

[5]Regenerative Medicine Center, University Medical Center Utrecht, 3584 EA Utrecht, The Netherlands

Abstract

De novo blood vessel formation occurs through coalescence of endothelial cells (ECs) into a cord-like structure, followed by lumenization either through cell-[1–3] or cord-hollowing[4–7]. Vessels generated in this manner are restricted in diameter to 1 or 2 ECs, and these models fail to explain how vasculogenesis can form large diameter vessels. Here, we describe a model for large vessel formation that does not require a cord-like structure or a hollowing step. In this model, ECs coalesce into a network of struts in the future lumen of the vessel, a process dependent upon BMP signalling. The vessel wall forms around this network and consists initially of only a few patches of ECs. To withstand external forces and to maintain the shape of the vessel, strut formation traps erythrocytes into compartments to form a rigid structure. Struts gradually prune and ECs from struts migrate into and become part of the vessel wall. Experimental severing of struts resulted in vessel collapse, disturbed blood flow, and remodelling defects, demonstrating that struts enable the patency of large vessels during their formation.

Cord-hollowing during vasculogenesis can either occur through fusion of intracellular lumens, formed through pinocytosis, of ECs connected in a head-to-tail orientation[1–3]

or through the formation of an extracellular lumen between two ECs. This latter model depends upon apical-basal polarization of ECs, which leads to the rearrangement of cell-cell junctions to the periphery of the two adjacent ECs. Delivery of negatively charged glycoproteins to the apical side of the cells subsequently leads to the formation of a lumen between the two ECs through electrostatic repulsion[4,5]. Alternatively, this extracellular lumen could also result from apical exocytosis of vacuoles[6]. As a result, the diameter of these vessels is restricted to either 1 (intracellularly lumen) or 2 ECs (extracellular lumen). However, since vasculogenesis can result in the formation of large vessels, it raises the question of how these vessels acquire their large diameters. A good example of such a large diameter vessel is the posterior cardinal vein (PCV), which forms along with the dorsal aorta (DA) the first blood vessels in the developing vertebrate embryo. In zebrafish, the caudal portion of the PCV, posterior to the yolk sac extension, is referred to as the caudal vein (CV) and is approximately 5 times larger than the DA and thereby the largest blood vessel observed during development. Despite this large difference in diameter, the DA and PCV are formed and become functional over a nearly equivalent time-frame, suggesting that the lumen of the CV is likely not formed by one of the currently known mechanisms. To investigate how the CV is formed, we visualized its formation from 18 hours post fertilization (hpf) onwards, the timepoint when ECs start to form the DA and CV at the midline of the embryo[8]. For visualization purposes, we focused either on the area of lumen formation (Fig. 1a; orange box) or vessel wall formation (Fig 1a; green box). Around 18 hpf, the most medially positioned ECs started to coalescence into a network spanning the future lumen of the CV (Fig. 1b; orange boxes and Supplementary Video 1 left panel). Most branches of this network are comprised of multiple ECs (Extended Data Fig. 1a). By time-lapse imaging, we found that this network gradually prunes and disappears from the lumen by 26–28 hpf (Fig. 1b (orange boxes), c (blue area), Extended Data Fig. 1b and Supplementary Video 1 left panel). The wall of the CV is comprised initially out of only a few patches of ECs (18 hpf), which is in stark contrast with the current models of vasculogenesis, in which the vascular cord already forms a "leak-proof" vessel before lumenization (Fig. 1b, green boxes and Supplementary Video 1 right panel). Since closure of the vessel wall coincided with pruning of the endothelial network, we hypothesized that ECs from the network are re-used to form the CV wall. To test this hypothesis, we traced ECs within individual branches of the network by ultraviolet photoconversion of the DENDRA2 fluorescent protein from green to red. We found that the majority of the converted ECs (in 17 out of 25 embryos) had integrated into the wall of the CV 20 hours after conversion (Fig. 1d). In roughly 30% of the cases we found converted cells integrate into the arterial system, with ECs integrated into the floor of the DA or as single cells in the sub-aortic space between the DA and PCV, a typical appearance of hematopoietic stem and progenitor cells (Fig. 1e)[9,10]. Thus, the CV is formed around a temporary network of both arterial and venous ECs which seems to maintains the patency of the CV. Hence, we termed these structures endothelial struts. Of note, we also found struts in the anterior part of the PCV, consisted only out of 1–2 ECs, which is consistent with the smaller diameter relative to the posterior CV (Extended Data Fig. 1c). Furthermore, we did not find any evidence of EC proliferation or apoptosis during the formation or pruning of struts, suggesting that through an intricate mechanism of EC coalescing into struts, pruning, and EC migration

large diameter blood vessels can be formed without the need for expanding the initial pool of ECs (Extended Data Fig. 1d).

Our photoconversion experiments suggested that struts in the CV contained arterial ECs (Fig. 1e). This finding is intriguing since arterial and venous precursors arise from two distinct locations in the lateral plate mesoderm and were hypothesized to form the DA and PCV as independent entities[11]. Our images from the trunk at 20 hpf, showed two separate populations in the anterior part of the trunk that become increasingly intermingled without a clear separation in the posterior part of the trunk (CV region) (Fig. 2a). The arterial and venous ECs in the CV region formed a common precursor vessel that over time unmixed into the DA and CV in an anteroposterior direction (Fig. 2b and Supplementary Video 2). We visualized arterial and venous ECs by imaging embryos in which arterial ECs were fluorescently labelled by the arterial-restricted Notch ligand *delta-like 4* (*dll4*)[12] or by fluorescent reporting of Notch activity (*Tp1*)[13]. Consistent with results from our photoconversion experiments, we found that some ECs in struts located within the CV expressed *dll4* or were positive for Notch activity (*Tp1*) (Fig. 2c and d). Of note, we observed that the majority of arterial ECs that were juxtaposed to the hypochord, forming the roof of the DA, had a higher GFP signal (*dll4*) and showed increased Notch activity (*Tp1*) compared to arterial ECs positioned more ventrally (Fig. 2c and d). These findings suggest that arterial ECs positioned against the hypochord have a stronger arterial signature than the more ventrally positioned arterial ECs, which include those forming endothelial struts. From this, we reasoned that unmixing of arterial and venous ECs in the CV occurs through the gradual increase of arterial genes in the more ventrally positioned arterial ECs, including struts. To test this, we inhibited arterial differentiation by abrogating Notch signalling through administration of the γ-secretase inhibitor DAPT[14]. In a complementary approach, we used a morpholino oligonucleotide to knock down the downstream Notch target *ephrinB2a* (*efnb2a*), which demarcates arterial and venous boundaries[15–17]. In both experiments, we found a dose-dependent inhibition of arterial-venous unmixing, resulting in a DA and PCV that remained fused (Fig. 2e, f and Extended Data Fig. 2a). The loss of Notch signalling in DAPT treated embryos was illustrated by the marked reduction of *dll4* expression, which we did not observed in *efnb2a* morphants, a down-stream Notch target gene (Fig. 2e; arrowheads). Importantly, inhibition of arterial specification did not affect strut formation or pruning (Extended Data Fig. 2b). Thus, a single precursor vessel is formed by arterial and venous ECs in the CV region, with struts of either EC type, that over time unmixes into the DA and CV through increasing expression of arterial genes like *efnb2a*.

Since Bone morphogenetic protein (BMP) plays a pivotal role in the remodelling of the CV into the caudal vein plexus, a process that starts after the CV becomes functional[18–20], we tested whether or not BMP signalling also plays a role in strut formation. To this end, we inhibited BMP signalling by expressing the BMP antagonist *noggin* via a *Tg(hsp70:noggin)* trangene[19] or treatment with the small molecule DMH1, a dorsomorphin analogue[21]. Alternatively, we ectopically activated the bmp pathway by expressing *bmp2b* via the *Tg(hsp70:bmp2b)* transgene[22]. *Noggin* and *bmp2b* expression were controlled by the heat-shock inducible promoter (*hsp70*) and thereby allowed for manipulation of BMP signalling after the BMP-dependent specification of dorsoventral mesoderm[23,24]. Genetic or chemical inhibition of BMP signalling from 16 hpf onwards resulted in a failure of the ECs to

coalescence into struts (Fig. 3a). Next, we ectopically expressed *bmp2b* from 16 hpf onwards and found that a portion of the struts were still present at 48 hpf (Fig. 3b; upper panels), whereas in wildtype embryos all struts were cleared from the lumen by 26–28 hpf (Fig. 1b and c). In addition, we found that the CV wall in these embryos was only partially formed (Fig. 3b asterisk, c and Supplementary Video 3). This may be explained by the inability of ECs in struts to migrate into the CV wall. Ectopic expression of *bmp2b* between 18–22 hpf disrupts cardiac morphogenesis[22] and to circumvent this cardiac phenotype we heat-shocked around 22 hpf. Of note, at this time, the majority of the struts have already been pruned and therefore we could only target the few remaining struts (Fig. 1b, c). Similar to the experiments performed at 16 hpf, we also found struts that persisted at 48 hpf while heart formation and circulation showed no obvious defects (Fig. 3b; lower panels). In addition, these embryos also displayed a previously described ectopic sprouting phenotype (Fig. 3b; lower panel arrows)[19]. Bmp2b regulates cellular responses through interaction with BMP-receptors type I and II, resulting in the phosphorylation of Smads 1, 5, and 8 (R-Smads), followed by heterodimerization of these phosphorylated R-Smads with co-Smad4 and ultimately the regulation of a myriad of downstream transcriptional targets, like the angiogenic factor *id1*[25–27]. To further test whether strut formation was facilitated through this canonical BMP pathway, we generated a constitutively active zebrafish Smad1 (caSmad1), placed under the control of the endothelial specific promoter fli1a and injected it at the single cell stage for mosaic expression[28–30]. Similar to the ectopic expression of *bmp2b,* caSmad1-mCLover positive struts failed to prune and were still present at 48 hpf, while injections of mClover alone did not prevent pruning of struts (Fig. 3d and Extended Data Fig. 3a). By using a bmp reporter *Tg(bre:eGFP)*, we found that besides expression in epidermal cells and erythrocytes, ECs in struts have active bmp signalling at different stages of CV formation (Fig. 3e)[31]. This is further supported by the presence of mRNA transcripts of both bmp2b receptors (*bmpr2a* and *bmpr2b*) and the downstream bmp target *id1*, indicative of active bmp signalling, in sorted ECs from the CV (Extended Data Fig. 3b). Thus, there is a temporal window in which bmp signalling is required for the formation of EC struts in the CV; prolonging this window via ectopic activation of bmp signalling prevents struts from pruning.

Pruning of endothelial struts coincides with the onset of blood flow, an important factor in vascular remodelling and endothelial cell fate determination[32–34]. To study blood flow in relation to endothelial struts, we simultaneously visualized erythrocytes and ECs during strut formation. At the onset of strut formation, erythrocytes were partially positioned between arterial and venous ECs and a large portion of the erythrocytes were mixed with venous ECs, especially in the CV region (Fig. 4a). As a result of this mixing, strut formation in the CV region trapped these erythrocytes into compartments, with some tightly packed with erythrocytes (Fig. 4b). The DA is initially devoid of erythrocytes (Fig. 4a and b (20 hpf)) and they only start to enter the DA when blood flow is initiated (Fig. 4b (24 hpf)). While initially trapped in these compartments, erythrocytes are gradually released into the circulation when struts start to prune, resulting in progressive loss of these compartments (Fig. 4c and Supplementary Video 4). Erythrocytes have been shown to be a source of secreted growth factors and since they are closely associated with the ECs prior strut formation, we questioned whether erythrocytes may be a source of *bmp2b* that contributes

to strut formation[35]. To test this, we first FACS sorted erythrocytes at the time of CV formation and found *bmp2b* expression by qPCR (Fig. 4d an Extended Data Fig. 4a). Of note, *bmp2b* is also expressed by the ventral mesoderm surrounding the CV, which is included in the unsorted population that we used as a reference[19]. Next, we prevented erythrocytes from leaving the CV by inhibiting the onset of circulation by either blocking the expression of *cardiac troponin T2a* (*tnnt2a*) or through administration of the muscle relaxant ms-222 (tricaine methanesulfonate). From these embryos, we dissected the CV region and measured a 2-fold increase in *bmp2b* expression, further supporting that the erythrocytes are a significant source of *bmp2b* (Fig. 4e). While we found no difference in the number of struts just before the onset of circulation (26 hpf), at 48 hpf we still observed the same number of struts than at 26 hpf in embryos without circulation (Fig. 4f and Extended Data Fig. 4b). Furthermore, in these embryos the CV wall was also not fully formed, which is in line with our earlier findings that ECs from struts are re-used to form the CV wall (Extended Data 4c; asterisks). In sum, we demonstrate that the erythrocytes secrete Bmp2b that is required for strut formation, become trapped in compartments formed by struts and gradually enter circulation when these compartments are progressively lost through pruning of struts.

To test the functionality of struts, we ablated 1–2 cells within a single strut by ultrashort pulses of near-infrared laser light, which was sufficient to severe the strut. This technique has been shown to generate negligible heat transfer and collateral damage to neighbouring tissues[36]. Due to the anatomical structure of the CV, we could only reliably sever endothelial struts after 22–24 hpf (Fig. 5a and Supplementary Video 5). While struts perpendicular to the sagittal plane were often difficult to detect and sever, we were able to ablate on average 95% of all struts within the CV (Fig. 5a; arrowhead middle right panel and Supplementary Video 6). As a control, we sham treated embryos by positioning the laser 25–50 microns next to struts, in the empty space of the lumen, with the same number of ablation pulses as in treated embryos. Severing of nearly all endothelial struts initially did not lead to a dramatic change in the shape of the lumen, however, at the onset of circulation, the lumen of the CV collapsed due to a nearly instantaneous removal of the erythrocytes from the CV (Fig. 5b, Extended Data Fig. 5a and Supplementary Video 7). This collapsed CV is severely mis-patterned during the remodelling of the CV into the CV plexus, although it allowed some blood flow (Fig. 5c). In animals in which circulation just had initiated, ablating a single strut often resulted in the release of erythrocytes into the circulation, demonstrating that these compartments trap erythrocytes (Supplementary Video 5; embryo 2).

In sum, we show that strut formation traps erythrocytes into compartments, with some tightly packed with erythrocytes, and forms thereby a rigid network that withstands external forces and maintains the shape of the vessel. Pruning of struts occurs gradually, ensuring that not all erythrocytes simultaneously enter the circulation, which would result in the collapse of the vessel (Extended Data Fig. 5b).

Methods

Zebrafish husbandry

Zebrafish (Danio rerio) were maintained and propagated according to the guidelines of the UCSD Institutional Animal Care and Use Committee and Hubrecht Institute ethical review board. All animal experiments were approved by the Animal Experimentation Committee (DEC) of the Royal Netherlands Academy of Arts and Sciences. Embryos and adult fish were raised in a circulating aquarium system (Aquaneering) at 28 °C. The following zebrafish lines have been previously described: *Tg(fli1a:lifeactCherry)*[ncv7Tg][18] referred to as fli1a:laCherry; *Tg(fli1a:eGFP)*[y1][30]; *Tg(hbbe1.1:EGFP)*[zf446][37] referred to as *Tg(globin:eGFP); Tg(flk:DENDRA2)*[38]; *Tg(dll4:Gal4FF)*[hu10049Tg][12]; *Tg(UAS:lifeactGFP)*[mu271][35] referred to as UAS:laGFP; *Tg(EPV.Tp1-Mmu.Hbb:GFP-utrn)* [13] referred to as *Tg(Tp1:GFP)*, *Tg(hsp70:bmp2b)* [fr13][22], *Tg(kdrl:nlsGFP)*[ubs1][6]. Details on the strains and ages are noted for each experiment. Gender was not selected in any of the studies conducted.

Morpholino, plasmid injections, heat-shock and chemical treatment

Embryos were injected at the one-cell stage with morpholino oligonucleotides (MOs; GeneTools) or 50 ng plasmid with 100ng *tol2* mRNA. Ephrinb2a (efnb2a) translation blocking MO (5′- CGGTCAAATTCCGTTTCGCGGGA-3′)[39]; Silent heart morpholino *tnnt2a* (5′-CATGTTTGCTCTGATCTGACACGCA-3′)[40]. Scrambled MO was injected at similar concentrations as the targeted MO (5′-CCTCTTACCTCAGTTACAATTTATA-3′). Capped tol2 mRNA was synthesized from linearized pCS2+ constructs using the mMessage mMachine SP6 kit (Ambion, AM1340). Injected and un-injected control embryos were heat-shocked at 38 °C for 30 minutes. Embryos were treated with 50 μM DMH1 (#16679, Cayman Chemical), 40 μM DAPT (#13197, Cayman Chemical) dissolved in DMSO (1000X stock solution) and control embryos were treated with DMSO alone. Blood flow was inhibited by treating the embryos with 0.48 mg/ml (3x) Ethyl 3-aminobenzoate methanesulfonate (MS222; sigma E10521). Live embryos were soaked in 10 μg/ml (Thermofisher A1301) dissolved in E3 medium for 30 minutes and extensively washed with E3 medium afterwards and subsequently imaged.

Microscopy and laser ablation

Live microscopy was done in environmentally controlled microscopy systems based on a Leica TCS SP5 or SP8 confocal microscope or a Zeiss LSM 880 with Airyscan. For all imaging, embryos were placed into a modified Four-Well WillCo dish[41] submerged in E3 medium containing 0.168 mg/ml = 0.0168% = ~0.02% Ethyl 3-aminobenzoate methanesulfonate (MS222; sigma E10521) at a temperature of 28.5 °C. Imaging was subsequently done with either 20x/0.75, 40x/1.4 or 63x/1.46 objectives.

For laser ablation experiments, embryos were embedded in 1% low melting point agarose (Invitrogen) in a WillCo dish with a 40 mm #1.5 cover glass bottom and placed under a two-photon laser scanning microscope of local design that included an amplified beam[42]. Laser ablation of endothelial struts was achieved by using targeted ultra-fast laser pulses that were generated with a multi-pass Ti:Al2O3 amplifier of local construction that followed

a previously published design[36] and operated at a 5 kHz pulse-rate. The Ablation beam and the imaging beam were combined before the microscope objective with a polarizing beam splitter[36]. We focused the two beams in the same focal plane and centred the ablation beam in the area that is raster-scanned by the imaging beam so that ablation occurred at the centre of the TPLSM imaging field. The energy per pulse of the ablation beam was tuned with neutral density filters and the number of pulses was controlled by a mechanical shutter (Uniblitz LS3Z2 shutter and VMM-D1 driver; Vincent). The energy and number of pulses was modified based on damage assessed from the real-time TPLSM images. Ablation was carried out with 25 pulses of 0.2μJ delivered at 5 kHz

Cloning

The coding sequence of zebrafish Smad1 (ENSDARG00000027199) was cloned into the pCS2+ vector by the Gibson Cloning method (NEB HiFi DNA Assembly mix, E2621S). To substitute serine 470 and 472 into aspartic acid (SVS to DVD), zfSmad1 was subcloned with reversed primers containing the required nucleotide changes (see supplemental table for primer sequence) and fused to mClover3 (N-terminally) spaced with the flexible linker GSAGSAAGSGEF in front of the fli1a endothelial specific promoter, referred to as *Tg(fli1a:mClover-caSmad1)*. The coding sequence of Ephrinb2a (ENSDARG00000020164) was cloned into the pCS2+ vector and mRNA was transcribed with the Sp6 message machine kit (Promega).

Cell preparation and flow cytometry

Embryos were collected and anesthetized in E3 medium containing 0.01% tricaine the CV region or trunk region was dissected and placed in ice-cold PBS. After centrifugation the pellet was washed with ice-cold PBS and resuspended TrypLE (ThermoFisher, 12563011) for 45min at 32 °C with vigorous shaking. Cells were then washed with FACS buffer (PBS + 2% FBS + 2mM EDTA), dissolved in FACS buffer + DAPI (ThermoFisher, 0.5ug/ml final concentration) and subsequently filtered through 40-μm nylon mesh. Cells were sorted on a FACS Aria II (BD Biosciences) and collected in FACS buffer for gene expression analysis. FSC and SSC were cut of 50K, live cells were DAPI negative ($< 5 \times 10^2$). Gating strategy for erythrocytes (GFP) and endothelial cells (mCHerry) are shown in Extended Data Fig. 3b and 4a.

qPCR and RT–PCR

RNA was extracted from dissected tissue (CV region) or sorted cells by using Trizol (ThermoFisher) according to the manufacturer's instructions. cDNA was generated by using GoScript (Promega) using random hexamer primers. Quantitative real-time PCR (qPCR) assays were performed on a BIO-RAD CFX96 real time system according to the manufacturer's instructions (BIO-RAD) with Fast SYBR Green (Biorad,). The expression of ef1a, 18s, tbp and bactin were used to normalize the amount of the investigated transcripts. Primers used are listed in Supplemental Table 1.

Imaging

Images captured in aryscan mode (ZEISS LSM880 with ZEISS ZEN blue version 3.0) were first processed in ZEISS ZEN blue (aryscan processing) and subsequent analysed using FIJI (version 1.52P) or Imaris (version 9.1). Sub-stacks were subtracted to specifically visualize the blood vessel wall or lumen or Z-stacks were flattened by maximum intensity projection, method used is stated in figure captions. In some cases, XY drifts were corrected using the MultiStackReg plugin (FIJI; B. Busse, NICHD, version (1.15)) and correction of fluorescence bleaching by Histogram Matching (FIJI). Tiled images were stitched with either ZEN blue or Imaris sticher (version 9.1) Contrast in all images was adjusted, Look Up Tables (LUT) adjusted (red to magenta or red/green to black and white) in FIJI or Imaris for visualization purposes. Surface renderings were performed in Imaris. Figure, movies and animations were created with Adobe Illustrator, Photoshop, After Effects and Premier (version CS5).

Reagents

A list of reagents and catalogue numbers is available in Supplementary Table 2.

## Statistical analysis and experimental setup

For each in vivo experiment, animals from the same clutch were divided into different treatment groups without any bias. The whole clutch was excluded if more than 10% of control embryos displayed obvious developmental defects. If necessary, statistical analysis was performed using SPSS version 20 (IBM). Mann–Whitney U test was used for statistical analysis of two groups, unequal variances. Unpaired t-test was used for two groups, equal variances. Kruskal-Wallis test was used for statistical analysis of multiple groups, equal variances, and 1-way ANOVA, for multiple groups, unequal variances. Dunn's post-hoc test was used for pairwise multiple comparisons. All experiments are a representation of at least two independent repeats.

Data availability

All data supporting the findings of this study are available from the corresponding author on reasonable request.
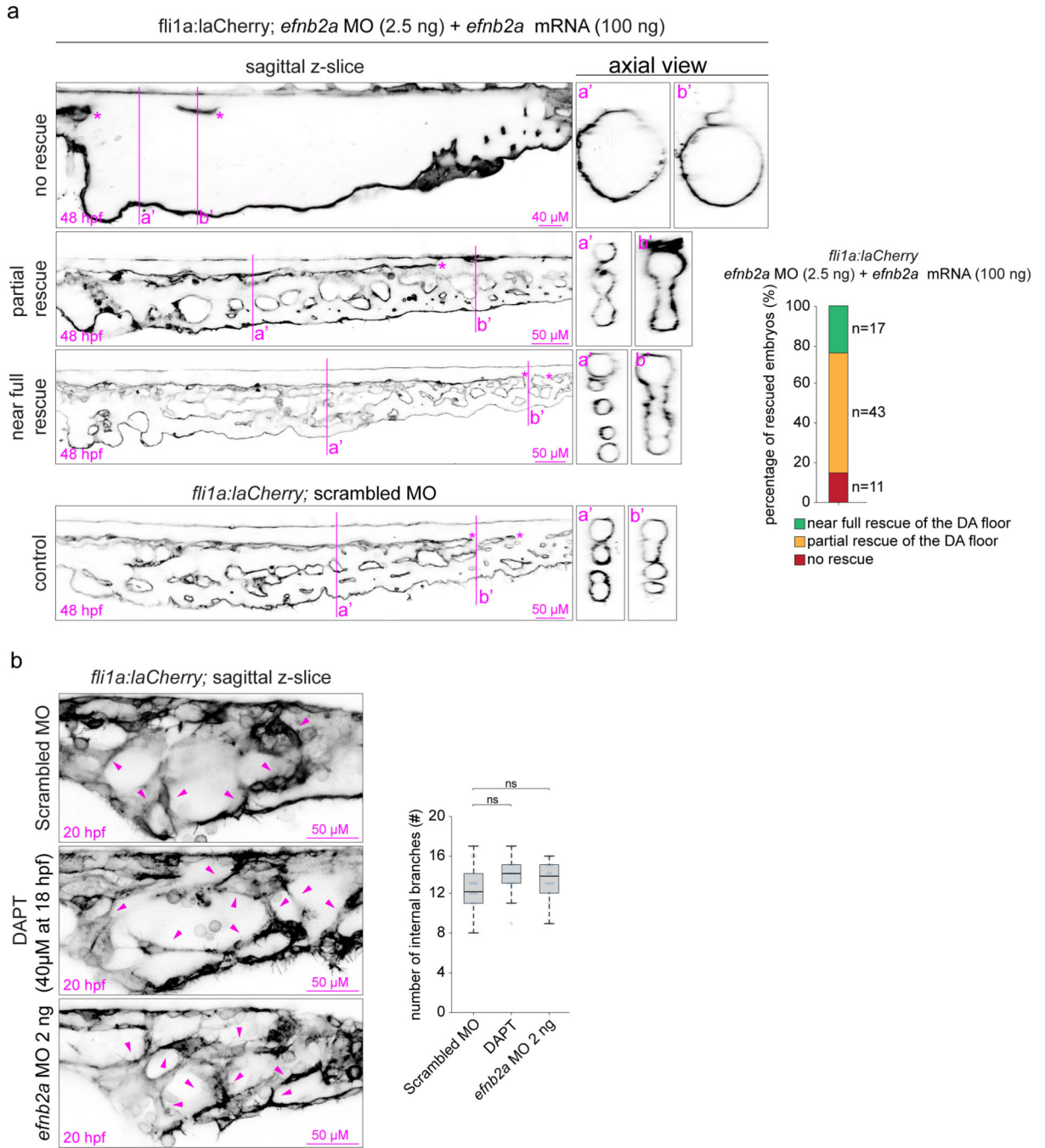
Extended Data

a

b

c

d
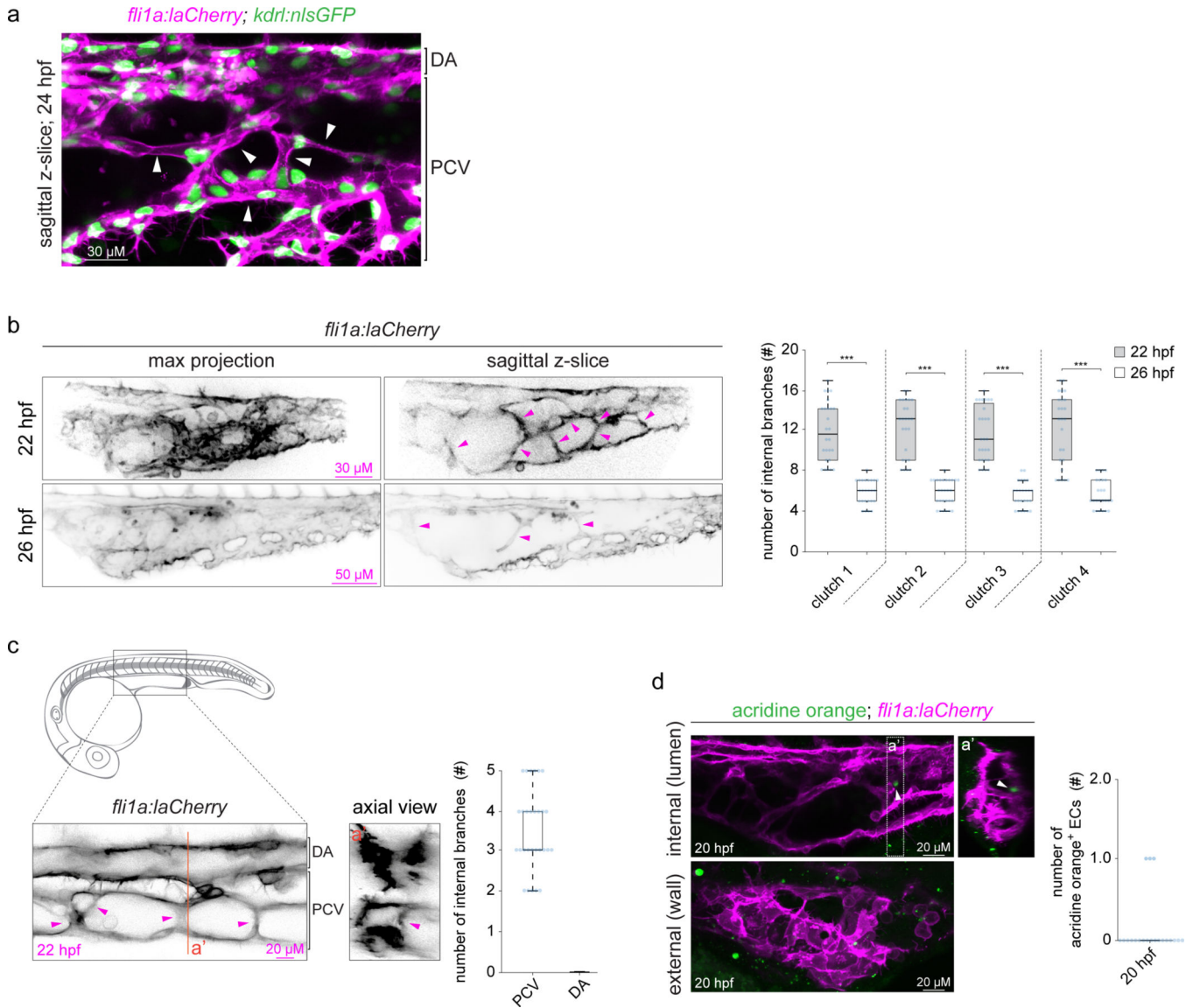
Extended Data Fig. 1. Characterization of endothelial struts.
(a) All ECs are marked by both laCherry (magenta; cytoskeleton) and eGFP (green; nuclei). Struts are depicted by arrowheads. Images are representative of 20 embryos analysed from two independent experiments. (b) Quantification of the number of endothelial struts at 22 hpf and 26 hpf by confocal microscopy and represented as the median values with the first and third quartiles; the whiskers represent the minimum and maximum (4 different clutches per time point (n=26; n=25; n=27; n=25 for 22 hpf and n=25; n=28; n=25; n=25 for 26 hpf. Two-tailed Student's *t*-test. ***P<0.0001* for all 4 tests). Arrowheads depict endothelial struts. Images are representative of indicated groups from four independent experiments. (c) Strut formation in the anterior part of the PCV at 22hpf by confocal microscopy and represented as the median values with the first and third quartiles; the whiskers represent the minimum and maximum (n=30 embryos from three independent experiments). Arrowheads

depict endothelial struts. (d) Quantification of the number of acridine orange positive ECs in the CV region at 20 hpf and representative confocal images. White arrowhead depicts a positive EC (n = 20 embryos from two independent experiments). Scale bars are defined in the figure.

Extended Data Fig. 2. Unmixing of arterial and venous endothelial cells.

(a) Rescue of ephrinb2a morphants with *efnb2a* mRNA. Embryos were grouped by the level of rescue (near full, partial or no rescue) of the floor of the DA, indicated by the asterisks.

(n= 71 embryos analysed in one experiment, n numbers per group indicated in graph). Images are representative of 5 embryos analysed by confocal microscopy per group. (b) Representative images and quantification of the number of struts in embryos treated with the Notch inhibitor DAPT or injected with an *ephnb2a* MO. As a control, embryos were injected with a scrambled MO. (n= 14 embryos per condition). Data presented as the median values with the first and third quartiles; the whiskers represent the minimum and maximum. Images are representative of 5 embryos analysed by confocal microscopy per condition. Scale bars are defined in the figure.
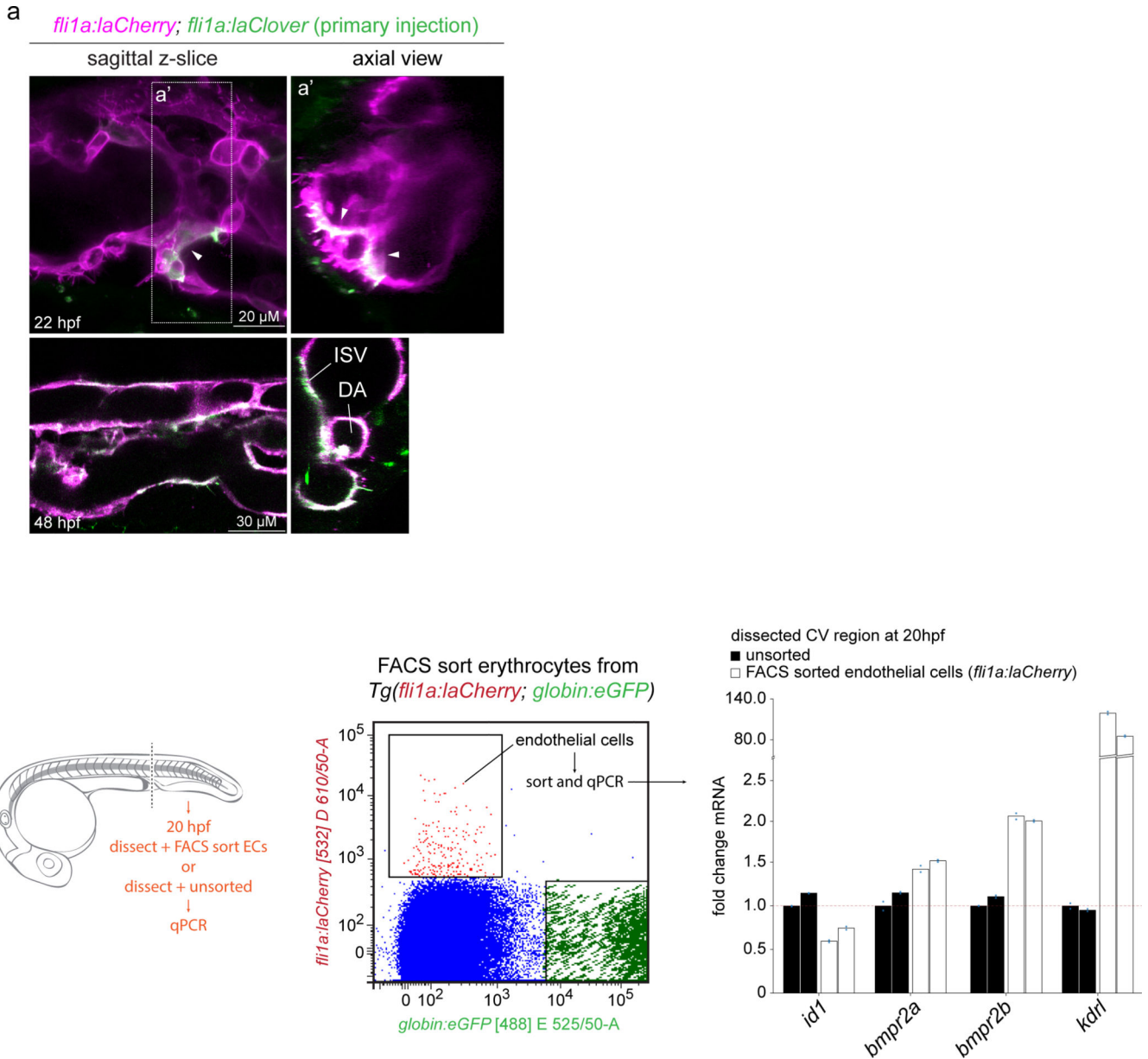
Extended Data Fig. 3. BMP signalling is required for strut formation.

(a) Mosaic expression of laClover under the control of the EC specific promoter *fli1a*. Arrowhead indicates mClover positive strut at 22 hpf (upper panel). Lower panel shows

an image of the same region at 48 hpf. Images are representative of 9 embryos analysed from three independent experiments. (b) Gating strategy used to FACS sort ECs from dissected CV regions followed by qPCR (10 CVs were pooled per condition measured in two independent experiments). Of note, the bmp pathway is active in multiple tissues at this time, including erythrocytes and strong activity in epithelial cells (Fig. 3e asterisks), these cells are included in the unsorted CV (black bars). Scale bars are defined in the figure.
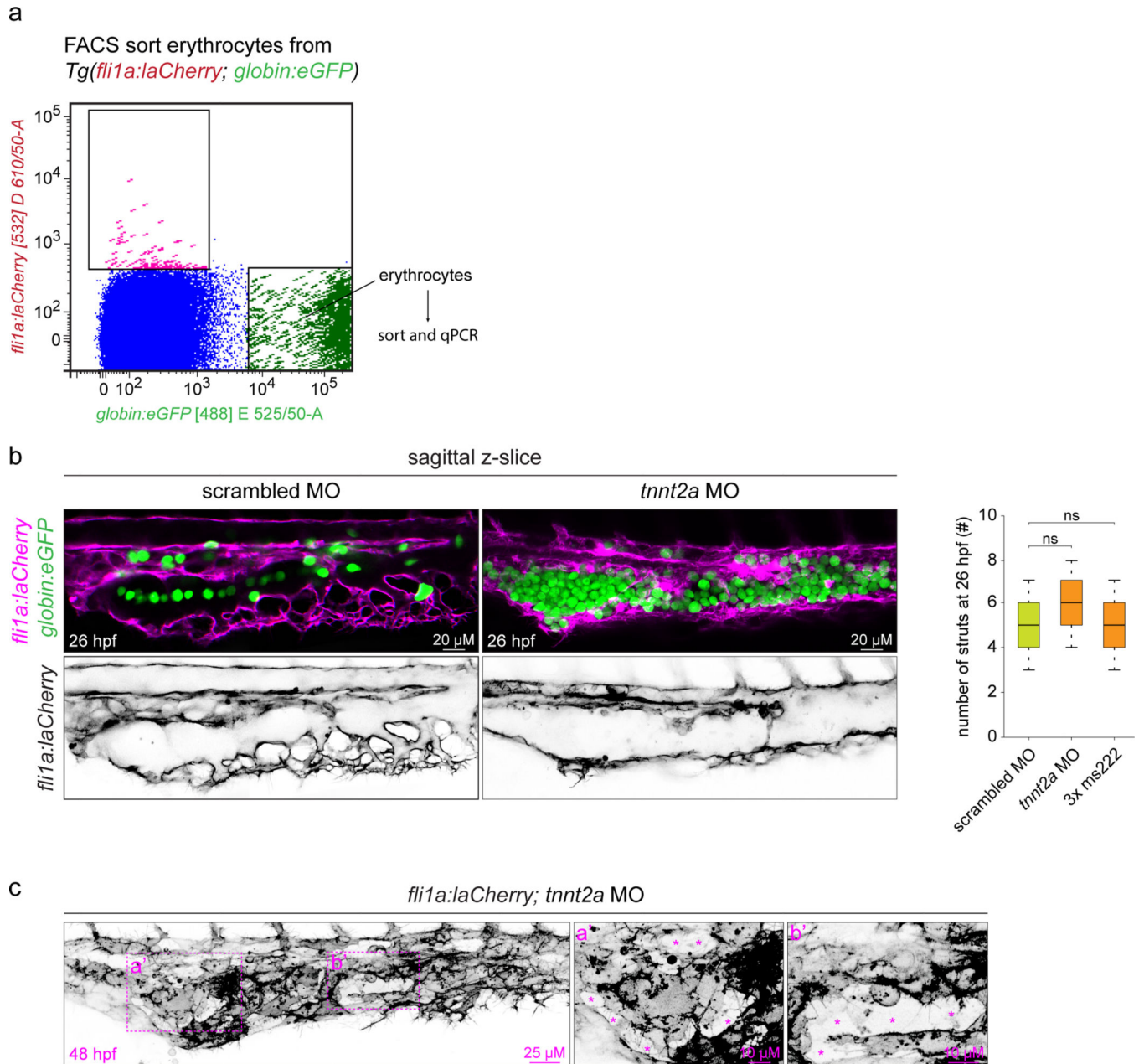
Extended Data Fig. 4. Inhibition of blood flow prevents struts from pruning.
(a) Gating strategy used to FACS sort ECs from dissected CV regions followed by qPCR (b) The onset of blood flow was inhibited by either injecting of a *cardiac troponin T2a* (*tnnt2a*) MO or through administration of 3x concentrated ms-222 (tricaine methanesulfonate).

Erythrocytes are marked by GFP (*globin*) and all ECs by laCherry (magenta). Data are presented as the median values with the first and third quartiles; the whiskers represent the minimum and maximum. One-way analysis of variance (ANOVA) with Dunn's post-hoc test. ns = not significant (n= 25 embryos per time points per experiment of three independent experiments). Images are representative of 5 embryos analysed by confocal microscopy per condition per experiment. (c) 48 hpf embryo injected with *tnnt2a* MO. Asterisks indicate an incomplete formation of the CV wall. Images are representative of 10 embryos analysed from two independent experiments. Scale bars are defined in the figure.
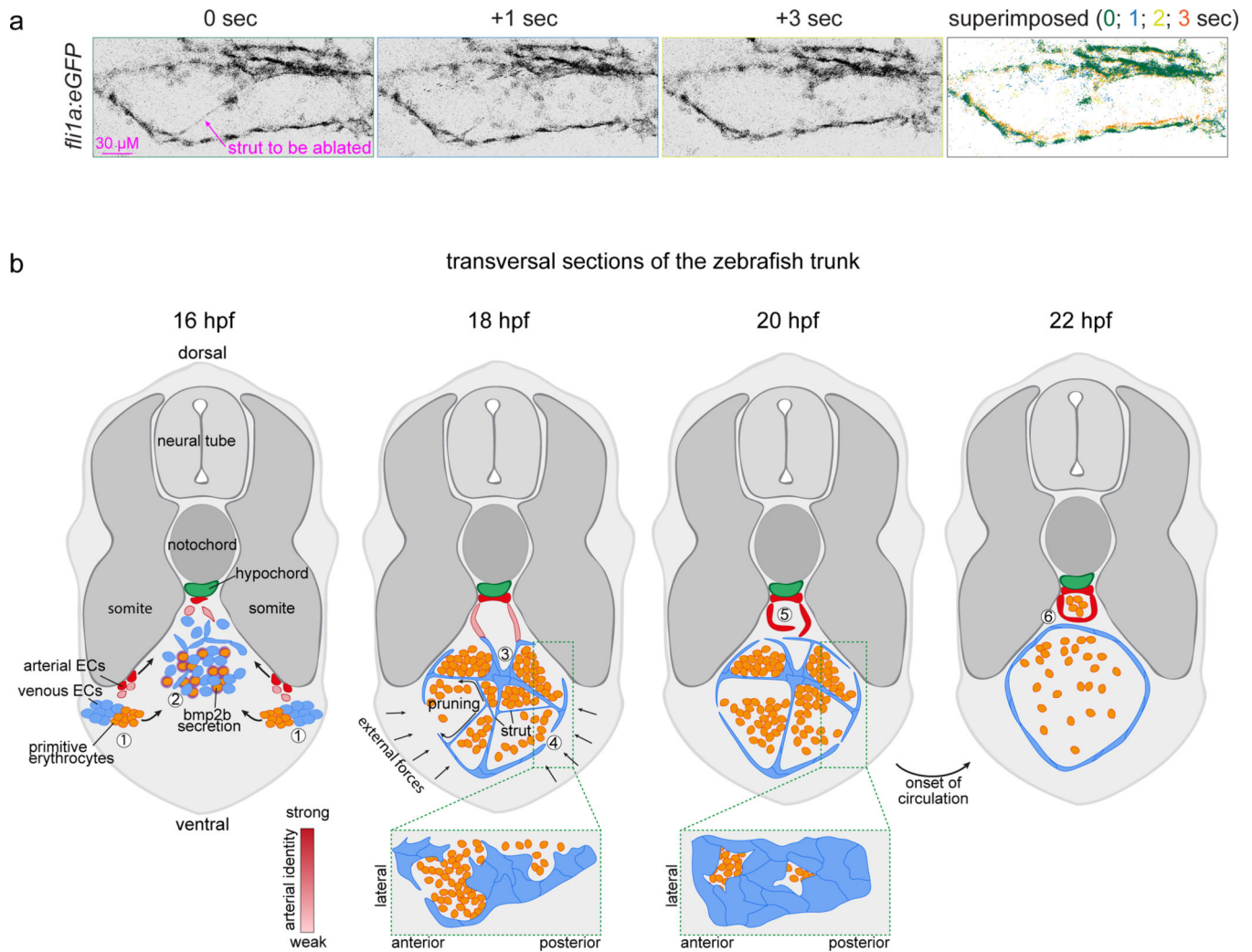
Extended Data Fig. 5. Endothelial strut model.

(a) Laser ablation of a single strut resulted in a slight deformation of the CV, shown by the superimposed image of all timepoints. Stills are representative of 18 embryos analysed from three independent experiments. Scale bar is defined in the figure (b) Schematic. **1**) Venous (blue) and arterial (red) EC precursors originate from distinct locations within the lateral plate mesoderm, with the primitive erythrocytes (precursors) positioned medially adjacent to the venous ECs. **2**) ECs and erythrocytes migrate towards the midline of the embryo. Arterial ECs migrate along and directly contact the ventral face of the somites,

thereby they receive inductive cues that strengthens the arterial fate (shades of red). **3**) At the midline, venous and arterial ECs coalesce into a network of struts and form a common precursor vessel. This process is bmp2b dependent, which is secreted by, among others, the erythrocytes. Strut formation encloses erythrocytes into compartments. **4**) The vessel wall consists initially only out of a few patches of ECs and upon pruning of struts, ECs from struts migrate into and are incorporated in the vessel wall. **5**) Arterial ECs participating in strut formation have a weak arterial identity, which progressively increases (shades of red) and results in the expression of the Notch target *efnb2b*, which drives the unmixing of arterial and venous ECs. Segregation of these arterial and venous ECs results in the formation of the DA and CV **6**) Onset of circulation flushes the *bmp2b* expressing erythrocytes from the CV, which is an important step for complete pruning of all struts. The lumen of the CV is now maintained by blood pressure rather than through the support of struts.

Supplementary Material

Refer to Web version on PubMed Central for supplementary material.

Acknowledgments

References

1. Folkman J. & Haudenschild C. Angiogenesis in vitro. Nature 288, 551–556 (1980). [PubMed: 6160403]

2. Kamei M. et al. Endothelial tubes assemble from intracellular vacuoles in vivo. Nature 442, 453–456 (2006). [PubMed: 16799567]

3. Davis GE & Bayless KJ An integrin and Rho GTPase-dependent pinocytic vacuole mechanism controls capillary lumen formation in collagen and fibrin matrices. Microcirculation 10, 27–44 (2003). [PubMed: 12610662]

4. Strili B. et al. Electrostatic cell-surface repulsion initiates lumen formation in developing blood vessels. Curr. Biol 20, 2003–2009 (2010). [PubMed: 20970336]

5. Ferrari A, Veligodskiy A, Berge U, Lucas MS & Kroschewski R. ROCK-mediated contractility, tight junctions and channels contribute to the conversion of a preapical patch into apical surface during isochoric lumen initiation. J. Cell Sci 121, 3649–3663 (2008). [PubMed: 18946028]

6. Blum Y. et al. Complex cell rearrangements during intersegmental vessel sprouting and vessel fusion in the zebrafish embryo. Dev. Biol 316, 312–322 (2008). [PubMed: 18342303]

7. Gebala V, Collins R, Geudens I, Phng L-K & Gerhardt H. Blood flow drives lumen formation by inverse membrane blebbing during angiogenesis in vivo. Nat. Cell Biol 18, 443–450 (2016). [PubMed: 26928868]

8. Hogan BM & Schulte-Merker S. How to plumb a pisces: understanding vascular development and disease using zebrafish embryos. Dev. Cell 42, 567–583 (2017). [PubMed: 28950100]

9. Bertrand JY et al. Haematopoietic stem cells derive directly from aortic endothelium during development. Nature 464, 108–111 (2010). [PubMed: 20154733]

10. Kissa K. & Herbomel P. Blood stem cells emerge from aortic endothelium by a novel type of cell transition. Nature 464, 112–115 (2010). [PubMed: 20154732]

11. Kohli V, Schumacher JA, Desai SP, Rehn K. & Sumanas S. Arterial and venous progenitors of the major axial vessels originate at distinct locations. Dev. Cell 25, 196–206 (2013). [PubMed: 23639444]

12. Hermkens DMA et al. Sox7 controls arterial specification in conjunction with hey2 and efnb2 function. Development 142, 1695–1704 (2015). [PubMed: 25834021]

13. Parsons MJ et al. Notch-responsive cells initiate the secondary transition in larval zebrafish pancreas. Mech. Dev 126, 898–912 (2009). [PubMed: 19595765]

14. Lawson ND et al. Notch signaling is required for arterial-venous differentiation during embryonic vascular development. Development 128, 3675–3683 (2001). [PubMed: 11585794]

15. Adams RH et al. Roles of ephrinB ligands and EphB receptors in cardiovascular development: demarcation of arterial/venous domains, vascular morphogenesis, and sprouting angiogenesis. Genes Dev. 13, 295–306 (1999). [PubMed: 9990854]

16. Wang HU, Chen ZF & Anderson DJ Molecular distinction and angiogenic interaction between embryonic arteries and veins revealed by ephrin-B2 and its receptor Eph-B4. Cell 93, 741–753 (1998). [PubMed: 9630219]

17. Herbert SP et al. Arterial-venous segregation by selective cell sprouting: an alternative mode of blood vessel formation. Science 326, 294–298 (2009). [PubMed: 19815777]

18. Wakayama Y, Fukuhara S, Ando K, Matsuda M. & Mochizuki N. Cdc42 mediates Bmp-induced sprouting angiogenesis through Fmnl3-driven assembly of endothelial filopodia in zebrafish. Dev. Cell 32, 109–122 (2015). [PubMed: 25584797]

19. Wiley DM et al. Distinct signalling pathways regulate sprouting angiogenesis from the dorsal aorta and the axial vein. Nat. Cell Biol 13, 686–692 (2011). [PubMed: 21572418]

20. Neal A. et al. Venous identity requires BMP signalling through ALK3. Nat. Commun 10, 453 (2019). [PubMed: 30692543]

21. Hao J. et al. In vivo structure-activity relationship study of dorsomorphin analogues identifies selective VEGF and BMP inhibitors. ACS Chem. Biol 5, 245–253 (2010). [PubMed: 20020776]

22. Chocron S, Verhoeven MC, Rentzsch F, Hammerschmidt M. & Bakkers J. Zebrafish Bmp4 regulates left-right asymmetry at two distinct developmental time points. Dev. Biol 305, 577–588 (2007). [PubMed: 17395172]

23. Mullins MC et al. Genes establishing dorsoventral pattern formation in the zebrafish embryo: the ventral specifying genes. Development 123, 81–93 (1996). [PubMed: 9007231]

24. Kishimoto Y, Lee KH, Zon L, Hammerschmidt M. & Schulte-Merker S. The molecular nature of zebrafish swirl: BMP2 function is essential during early dorsoventral patterning. Development 124, 4457–4466 (1997). [PubMed: 9409664]

25. Monteiro R. et al. Two novel type II receptors mediate BMP signalling and are required to establish left-right asymmetry in zebrafish. Dev. Biol 315, 55–71 (2008). [PubMed: 18222420]

26. Liu F. et al. A human Mad protein acting as a BMP-regulated transcriptional activator. Nature 381, 620–623 (1996). [PubMed: 8637600]

27. Lyden D. et al. Id1 and Id3 are required for neurogenesis, angiogenesis and vascularization of tumour xenografts. Nature 401, 670–677 (1999). [PubMed: 10537105]

28. Chen X, Zaro JL & Shen W-C Fusion protein linkers: property, design and functionality. Adv. Drug Deliv. Rev 65, 1357–1369 (2013). [PubMed: 23026637]

29. Kokabu S, Katagiri T, Yoda T. & Rosen V. Role of Smad phosphatases in BMP-Smad signaling axis-induced osteoblast differentiation. Journal of Oral Biosciences 54, 73–78 (2012).

30. Lawson ND & Weinstein BM In vivo imaging of embryonic vascular development using transgenic zebrafish. Dev. Biol 248, 307–318 (2002). [PubMed: 12167406]

31. Alexander C. et al. Combinatorial roles for BMPs and Endothelin 1 in patterning the dorsal-ventral axis of the craniofacial skeleton. Development 138, 5135–5146 (2011). [PubMed: 22031543]

32. Chen Q. et al. Haemodynamics-driven developmental pruning of brain vasculature in zebrafish. PLoS Biol. 10, e1001374 (2012).

33. Weijts B. et al. Blood flow-induced Notch activation and endothelial migration enable vascular remodeling in zebrafish embryos. Nat. Commun 9, 5314 (2018). [PubMed: 30552331]

34. Le Noble F. et al. Flow regulates arterial-venous differentiation in the chick embryo yolk sac. Development 131, 361–375 (2004). [PubMed: 14681188]

35. Helker CSM et al. The zebrafish common cardinal veins develop by a novel mechanism: lumen ensheathment. Development 140, 2776–2786 (2013). [PubMed: 23698350]

36. Nishimura N. et al. Targeted insult to subsurface cortical blood vessels using ultrashort laser pulses: three models of stroke. Nat. Methods 3, 99–108 (2006). [PubMed: 16432519]

37. Ganis JJ et al. Zebrafish globin switching occurs in two developmental stages and is controlled by the LCR. Dev. Biol 366, 185–194 (2012). [PubMed: 22537494]

38. Tian Y. et al. The first wave of T lymphopoiesis in zebrafish arises from aorta endothelium independent of hematopoietic stem cells. J. Exp. Med 214, 3347–3360 (2017). [PubMed: 28931624]

39. Cooke JE, Kemp HA & Moens CB EphA4 is required for cell adhesion and rhombomere-boundary formation in the zebrafish. Curr. Biol 15, 536–542 (2005). [PubMed: 15797022]

40. Sehnert AJ et al. Cardiac troponin T is essential in sarcomere assembly and cardiac contractility. Nat. Genet 31, 106–110 (2002). [PubMed: 11967535]

41. Weijts B, Tkachenko E, Traver D. & Groisman A. A Four-Well Dish for High-Resolution Longitudinal Imaging of the Tail and Posterior Trunk of Larval Zebrafish. Zebrafish 14, 489–491 (2017). [PubMed: 28118101]

42. Tsai PS & Kleinfeld D. in In Vivo Optical Imaging of Brain Function (eds. Frostig RD, Frostig RD, Frostig RD & Frostig RD) (CRC Press/Taylor & Francis, 2009).
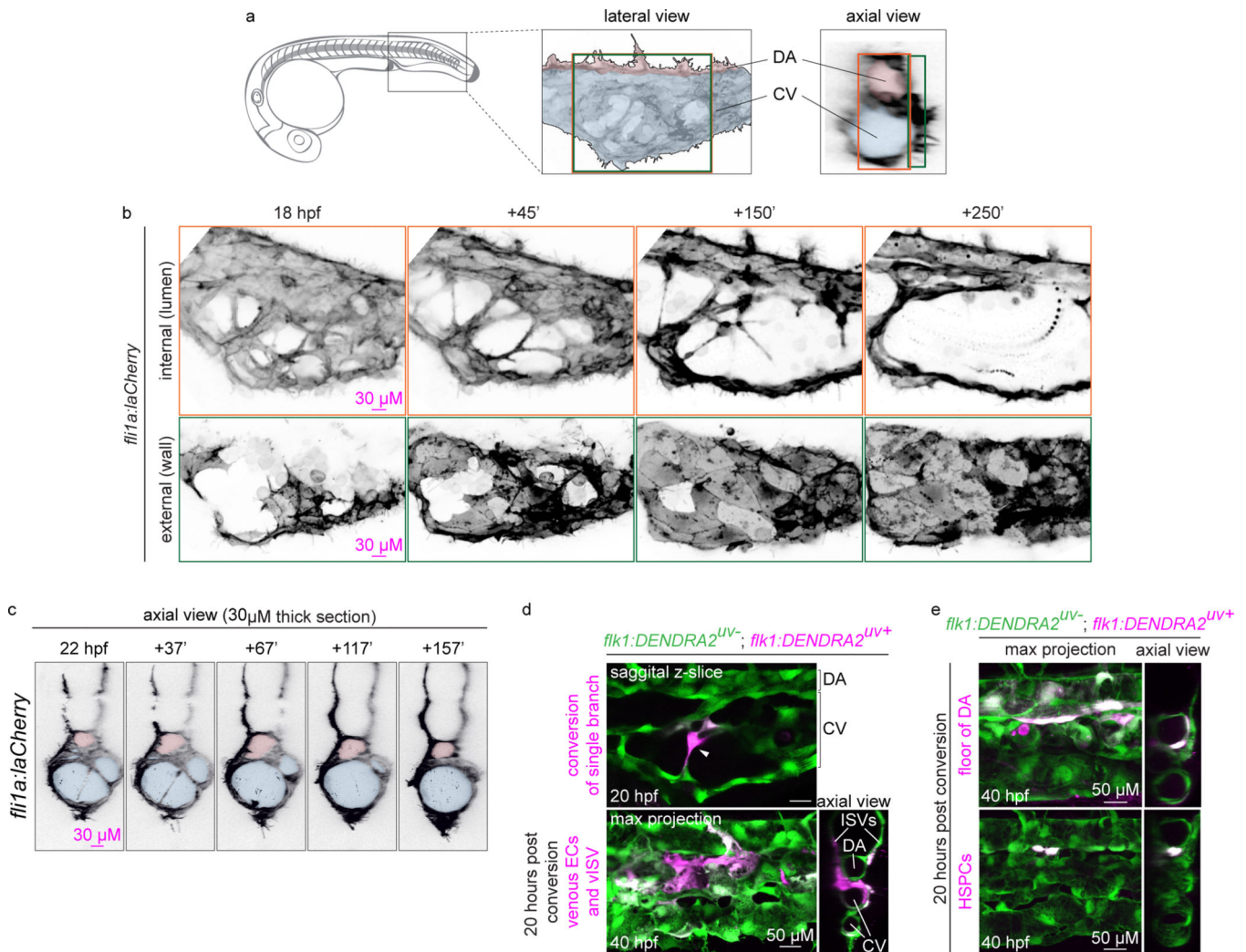
Figure 1. Formation of the caudal vein is facilitated through endothelial struts.
(a) Schematic representation of a 24 hpf embryo; orange (lumen) and green (vessel wall) boxes indicate visualized regions. Lumen of the DA and CV are pseudo-coloured by red and blue respectively. Anterior is orientated to the left for all imaging data in this study unless stated otherwise. Images are representative of 30 embryos analysed from three independent experiments. (b) Stills of Supplementary Video 1. Orange panel, ECs are labelled with lifeactCherry (laCherry) under the control of the endothelial specific promoter *fli1a*. Formation and pruning of endothelial struts within the future lumen of the CV. Green panel, formation of the vessel wall of the CV. Stills are representative of 5 independent time-lapse experiments in which each 1 embryo is imaged. (c) Axial view during the formation of the CV. Lumen of the DA and CV are pseudo-coloured in red and blue respectively. Images are representative of 25 embryos analysed. (d) Lineage tracing of ECs from struts by photoconversion of DENDRA2 (green-to-red). Images are representative of 30 embryos analysed from three independent experiments. In 70% of the embryos (17/25), the converted ECs were traced into the wall of the CV. White arrowhead depicts strut (e) In 30% of the cases, converted ECs were part of the floor of the DA (6/25) or the hematopoietic system
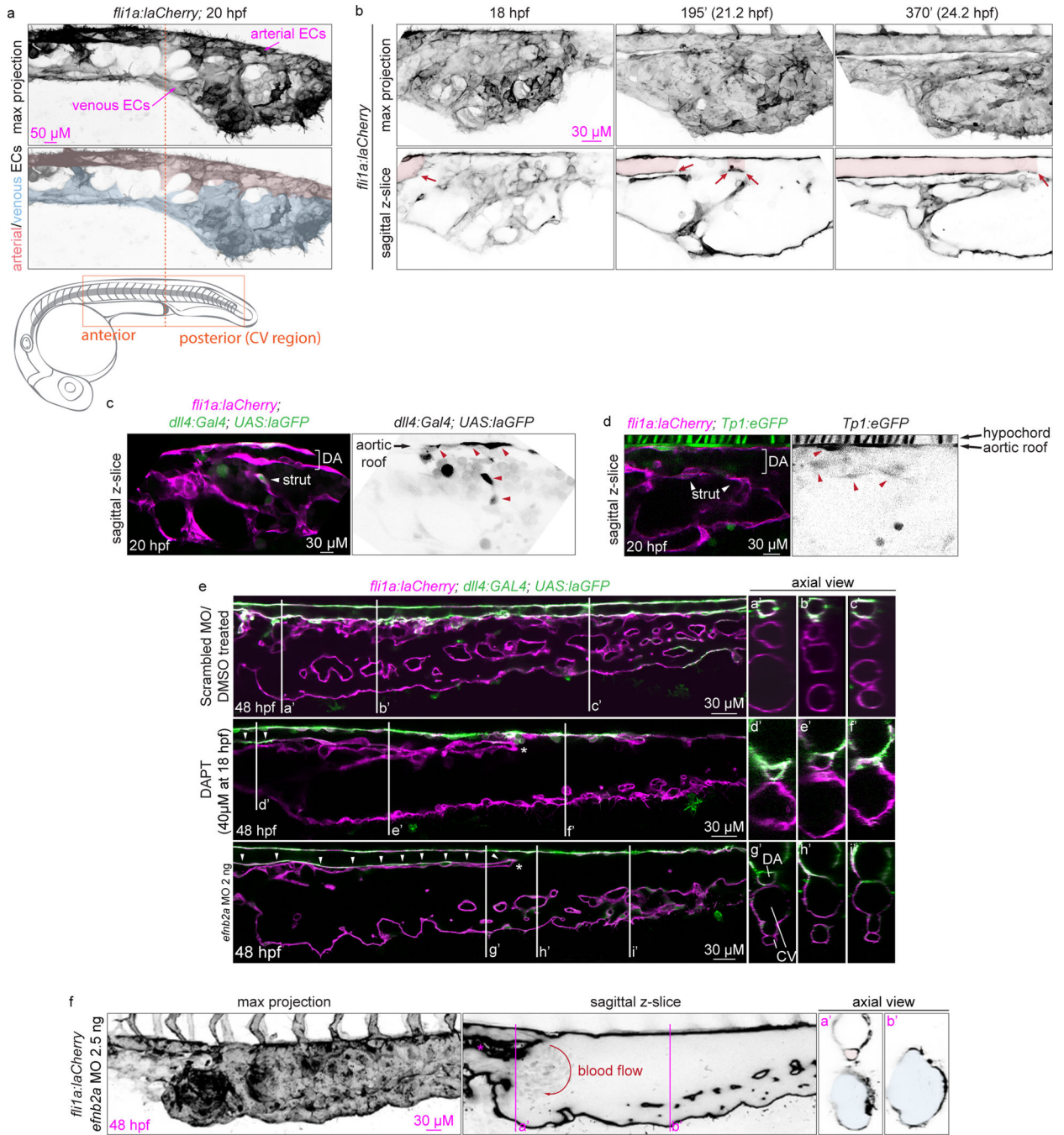
(hematopoietic stem and progenitor cells (HSPCs)) (2/25). Scale bars are defined in the figure.

Figure 2. The CV and DA arise from a common precursor vessel through unmixing of arterial and venous ECs.

(a) Arterial and venous EC populations are indicated by anatomical position. Right panel shows pseudo-coloured populations. Images are representative of 20 embryos analysed from two independent experiments. (b) Stills from Supplementary Video 2, the CV and DA are formed through segregation of arterial and venous ECs from a common pre-cursor vessel. Red colour and arrows depict the formation of the DA lumen. Stills are representative of 5 independent time-lapse experiments in which each 1 embryo is imaged. (c) Arterial ECs are marked by GFP (*dll4*; red arrowheads), all ECs are marked by laCherry (magenta)

and white arrowhead depicts strut. Images are representative of 20 embryos analysed from two independent experiments. (d) Notch signalling is reported by the expression of eGFP under the control of 12xCSL Notch responsive elements (*Tp1*, red arrowheads), all ECs are marked by laCherry (magenta) and white arrowheads depict struts. Images are representative of 20 embryos analysed from two independent experiments. (e) Chemical inhibition of the Notch signalling pathways by DAPT treatment or MO mediated knock-down of the downstream Notch target *ephrinb2a* in embryos in which arterial cells are marked by GFP (*dll4*) and all ECs by laCherry (magenta). As a control, a scrambled MO was injected at the same concentration as *efnb2a* MO or embryos were treated with the same concentration of DMSO in which the DAPT was dissolved. White arrowheads point at GFP (*dll4*) positive cells in the floor of the DA. Asterisks mark the disruption in arterial and venous unmixing. All images are representative of 20 embryos analysed of two independent experiments. (f) A higher dose of *efnb2a* MO than in e results in a more dramatic unmixing phenotype. Magenta asterisks show the disruption in arterial and venous unmixing and the red arrow show the direction of blood flow. Note how some erythrocytes have faint laCherry expression, enabling visualization of the circulation. Images are representative of 30 embryos analysed from three independent experiments. Scale bars are defined in the figure.
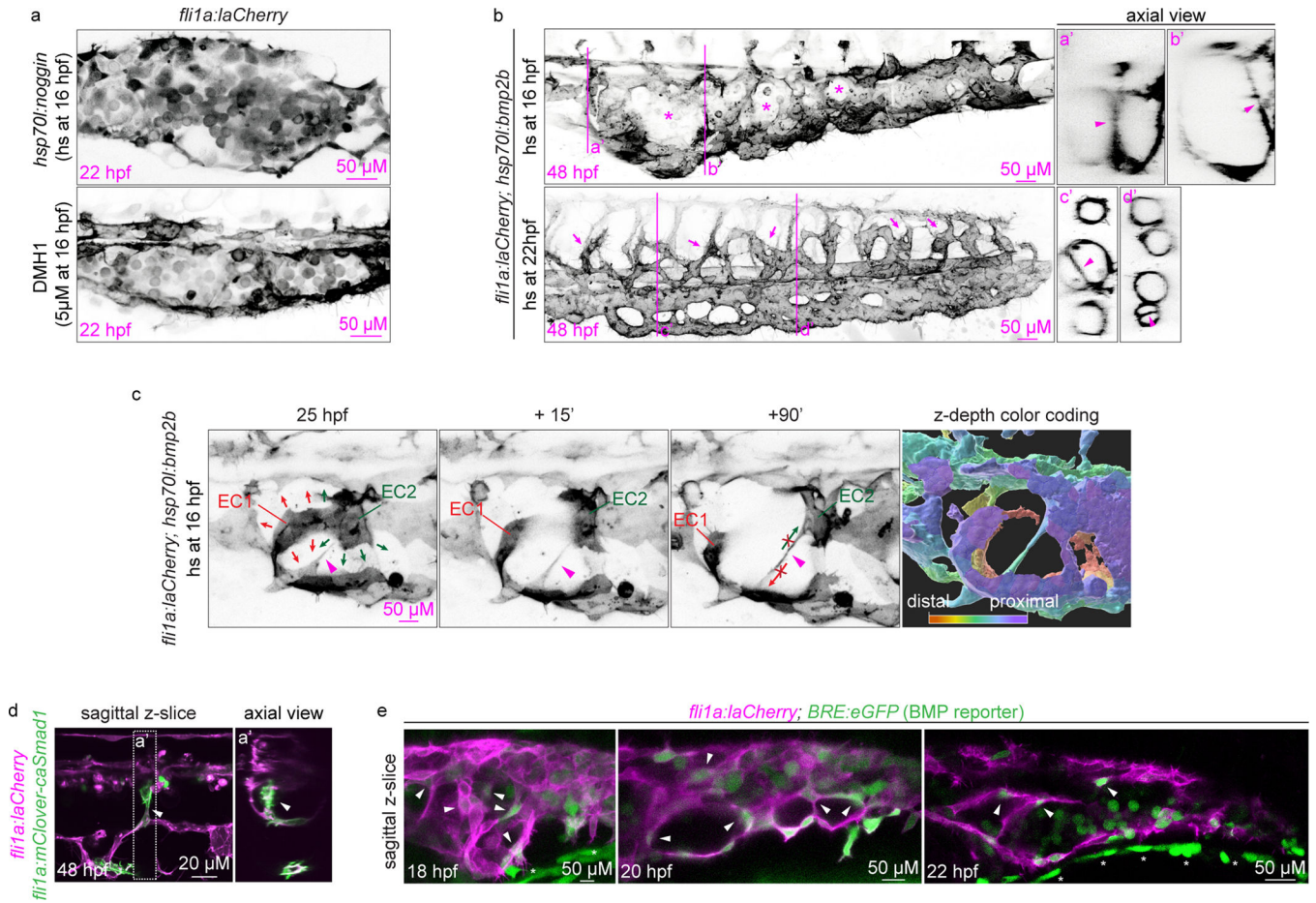
Figure 3. BMP signalling is required for strut formation.

(a) Inhibition of BMP signalling by heat-shock inducible expression of *noggin* (heats-hock at 16 hpf) or administration of 50 µM DMH1 from 16 hpf onwards. Images are representative of 20 embryos analysed from two independent experiments. (b) Ectopic expression of *bmp2b* by heat-shock at 16 hpf (upper panel) or 22 hpf (lower panel). Asterisks show a partially formed CV wall, arrowheads depict struts and arrows indicate a previous described venous sprouting phenotype[19]. Images are representative of 30 embryos analysed from three independent experiments. (c) Stills of Supplementary Video 3, ectopic expression of *bmp2b*, heat-shock at 16 hpf, prevents struts from pruning and consequently the closure of the vessel wall. Arrowheads depict struts and red and green arrows indicate the migration direction of two ECs. Last panel shows surface rendering with z-depth colour coding. Stills are representative of 2 independent time-lapse experiments in which each 1 embryo is imaged. (d) Constitutively active Smad1 fused to mClover (green) under the control of the EC specific promoter *fli1a* was injected for mosaic expression in *Tg(fli1a:laCherry)* embryos in which all ECs are marked by laCherry (magenta). Arrowheads depict mClover-caSmad positive strut. Images are representative of 30 embryos analysed from three independent experiments. (e) Different developmental stages of embryos in which all ECs are marked by laCherry (magenta) and Bmp activity is reported by eGFP. Arrowheads depict GFP positive struts. Note GFP positive erythrocytes within the CV region and the high expression of GFP by epithelial cells (asterisks). Images
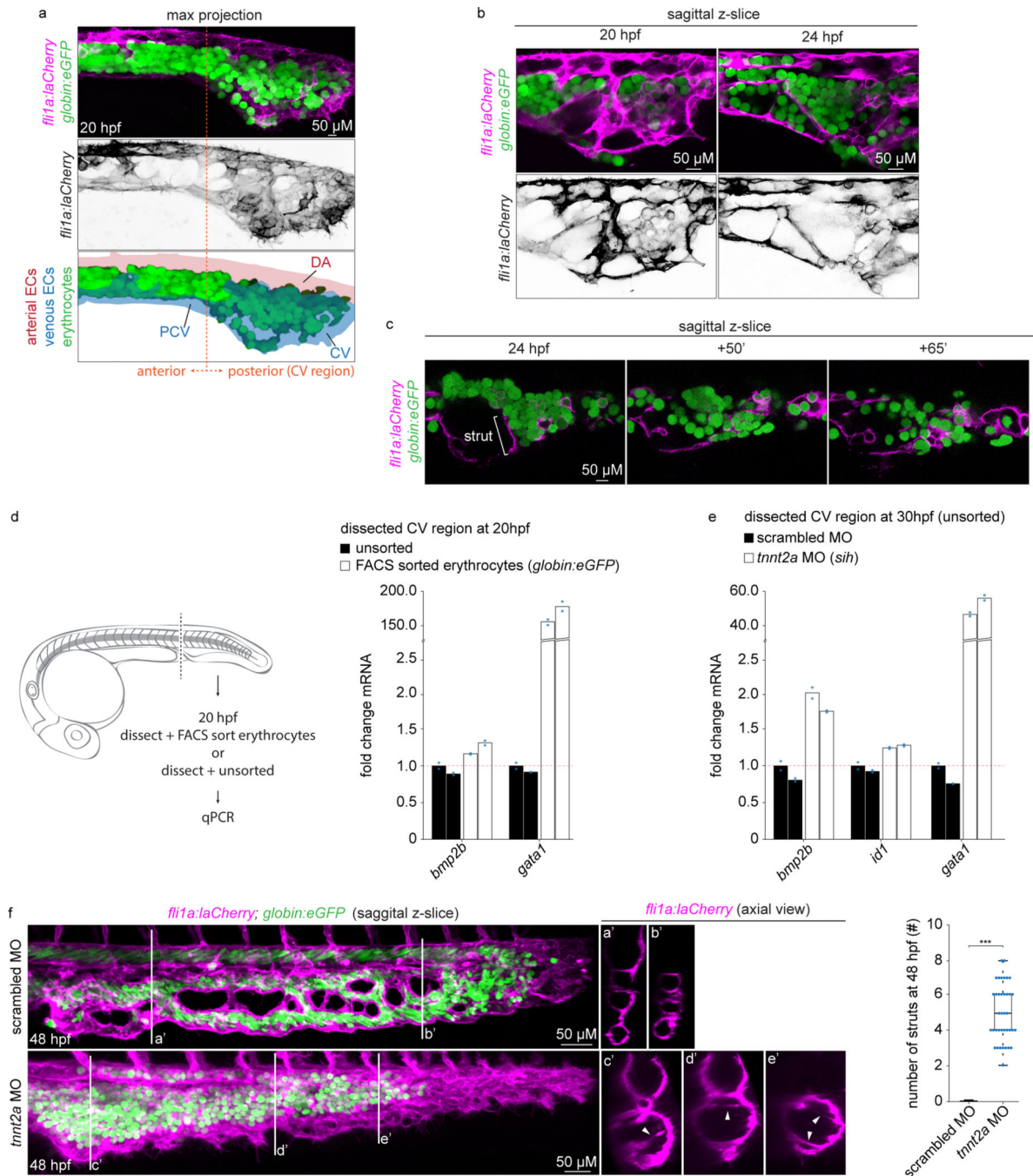
are representative of 20 embryos analysed from two independent experiments. Scale bars are defined in the figure.

Figure 4. Struts compartmentalize the CV and trap erythrocytes.
(a) Visualization of erythrocytes by eGFP (*globin*) and all ECs by laCherry (magenta)
in the trunk during strut formation. Images are representative of 30 embryos analysed
from three independent experiments. (b) Strut formation compartmentalizes the CV, thereby
trapping erythrocytes into compartments. Images are representative of 30 embryos analysed
from three independent experiments. (c) Stills of Supplementary Video 4, pruning of strut
results in the release of erythrocytes into the circulation. Stills are representative of 5
independent time-lapse experiments in which each 1 embryo is imaged. (d) Quantitative

PCR on dissected CV regions and FACS sorted erythrocytes (10 CVs were pooled per condition measured in two independent experiments). (e) Quantitative PCR on dissected CV regions from embryos injected with a scrambled MO or *tnnt2a* MO to prevent the onset of circulation (10 CVs were pooled per condition measured in two independent experiments). (f) Embryos injected with a scrambled MO or *tnnt2a* MO. Arrowheads depict struts that failed to prune. Images are representative of 20 embryos analysed from two independent experiments. Boxplot on the right shows the quantification of the number of struts at 48 hpf (n=15 for scrambled MO and n= 38 for *tnnt2a* MO injected; data are from two independent repeats and presented as the median values with the first and third quartiles; the whiskers represent the minimum and maximum. Two-tailed Student's *t*-test. ****P<0.0001*). Scale bars are defined in the figure.
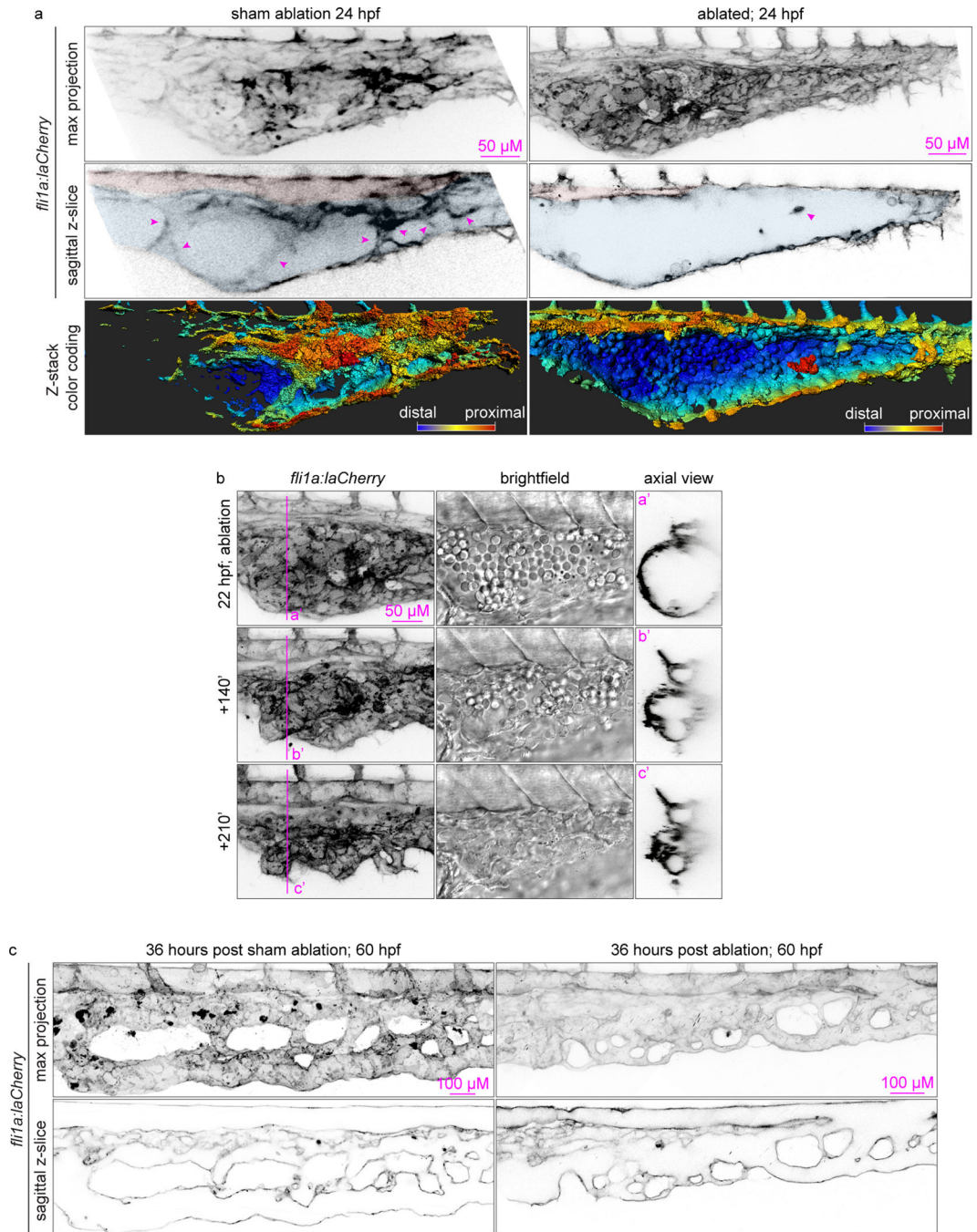
Figure 5. Endothelial struts provide structural support to the CV.
(a) Laser ablation of endothelial struts. In sham treated animals, the laser was fired ~25–50 microns next to the strut in the empty space of the lumen, with the same number of ablation pulses as in treated embryos. Ablation was carried out with 25 pulses of 0.2μJ delivered at 5kHz. Arrowheads depict struts. Lower panels show surface rendering with z-depth colour coding, the most distant cells are blue and cells at forefront are red. Images are representative of 18 embryos analysed from three independent experiments. (b) Stills of Supplementary Video 7, ablation of endothelial struts results in the collapse of the CV after

initiation of circulation. Stills are representative of 3 independent time-lapse experiments in which each 1 embryo is imaged. (c) Embryos 36 hours after sham treatment or laser ablation of struts. Images are representative of 18 embryos analysed from three independent experiments. Scale bars are defined in the figure.